ChemistrySelect

Research Article
doi.org/10.1002/slct.202305026

Chemistry Europe
European Chemical Societies Publishing

www.chemistryselect.org

Study on the Synthesis and Photocatalytic Performance of Modified TiO_2 Supported by G-C_3N_4 in the Degradation of 2,4-Dichlorophenoxyacetic Acid

Phung Thi Lan,*[a] Nguyen Hoang Hao,[b] and Le Minh Cam*[a, c]

The impact of alkaline hydrothermal treatment on the structure and morphology of Degussa P25 was evaluated. The modification results in a larger surface area, which improves 2,4-dichlorophenoxyacetic acid (2,4-D) adsorption capacity and has a remarkable effect on the 2,4-D photocatalytic degradation. The 30% mod. TiO_2/g-C_3N_4 and 50% mod.TiO_2/g-C_3N_4 composites were made by combining the treated Degussa P25 with g-C_3N_4 at mass ratios of 30% and 50%. Using XRD, SEM, EDX, BET, UV-vis DRS, and PL, the synthesized materials were physically characterized. When compared to their pure components, the composites show a longer "lifetime" of charge carriers and a reduced energy band gap. The 2,4-D degradation under visible light irradiation ($\lambda > 400$ nm) was used to assess their photocatalytic activity. The influence of pH and 2,4-D initial concentration were investigated. The enhanced 2,4-D degradation efficiency of more than 80% is ascribed to the cooperative photocatalytic action of mod.TiO_2 and g-C_3N_4. Both $^{\bullet}OH$, $O_2^{\bullet-}$ radicals and h^+ were the ROS dominating the degradation of 2,4-D under investigated experimental circumstances. The 2,4-D photocatalytic degradation follows pseudo-first order kinetics. The findings of this work indicate that Degussa P25/g-C_3N_4-based photocatalysts may be employed, depending on the pH conditions, in the wastewater treatment.

Introduction

The herbicide, which is one of the compounds that must be discussed, is the primary source of 2,4-D. Over the past decade, 2,4-D has been a commonly used herbicide for agricultural purposes. Because 2,4-D is highly mobile and poorly biodegradable so when sprayed on plants, it not only accumulates in the soil but it also disperses in surface water and groundwater. Furthermore, 2,4-D can be absorbed into the human body through inhalation, skin contact, or the gastrointestinal tract and is the main cause of cancer, birth defects, mutations, neurotoxicity, immunosuppression, cytotoxicity, and hepatotoxicity.[1] Therefore, efficient methods to remove 2,4-D are essential to improving the quality of land and water resources. Significant efforts including adsorption, coagulation-flocculation, biodegradation, and advanced oxidation processes have been developed to remove 2,4-D.[2–9]

[a] Dr. P. T. Lan, Prof. L. M. Cam
Faculty of Chemistry
Hanoi National University of Education
136 Xuan Thuy, Cau Giay, Hanoi, Vietnam
E-mail: lanpt@hnue.edu.vn
camlm@hnue.edu.vn

[b] Dr. N. H. Hao
College of Education
Vinh University
182 Le Duan, Vinh, Nghe An, Vietnam

[c] Prof. L. M. Cam
Faculty of Chemistry
Hanoi National University of Education
136 Xuan Thuy, Cau Giay, Hanoi, Vietnam
Thanh Do University
QL 32, Kim Chung, Hoai Duc, Ha Noi, Vietnam

Advanced oxidation with many advantages is being considered an effective method for the treatment of organic pollutants.[10,11] Currently, advanced oxidation using solar energy in combination with photocatalysts is used very effectively in decomposing pollutants in water,[12,13] reducing VOC emissions,[14] carbon dioxide,[15] and photolysis of water to produce clean energy such as hydrogen and oxygen,[16] etc. Numerous semiconductor nanomaterials have been studied.[17–21] Due to their high catalytic activity, high durability, and environmental friendliness, TiO_2-based photocatalysts are thought to have potential for the remediation of environmental contaminants. The limitation of TiO_2 is that TiO_2 possesses a poor solar energy conversion efficiency due to large energy bandgap (~3.2 eV), and a high recombination rate of photo-induced electron–hole pairs which results in low photocatalytic performance. Therefore, the photocatalytic activity of TiO_2 has not yet been achieved as per expectation. Several strategies, such as doping with metals[22] or non-metal,[23] coupling with visible-light active semiconductors,[24–27] etc have been addressed to tune its photocatalytic properties. Doping reduces the energy band gap, while coupling with other semiconductors enhance the separation rate of electron–hole pair charge through the transfer of electrons and holes between the semiconductors.[28] Among these strategies, combining it with another semiconductor of narrow energy band gap to create heterojunction proved to be beneficial.[25]

Graphite carbon nitride (g-C_3N_4), a non-metallic semiconductor material recently has attracted much attention because of its narrow bandgap (~2.7 eV), good mechanical durability, high chemical stability and being easy biodegradable.[29,30] However, the photocatalytic efficiency of g-C_3N_4 is hindered due to its low specific surface area (10–15 $m^2 g^{-1}$) which is

insufficient for visible - light absorption, and rapid recombination of photoinduced electron–hole pairs. These are the shortcomings that confine g-C_3N_4 to photocatalytic applications. More recently, several efforts have been undertaken to overcome its limitations, including co-catalysts incorporation, the construction of heterojunction, doping and the creation of composites with other semiconductor materials etc. Among these, heterojunction construction has shown to be beneficial since the delocalized conjugated π structure of the interface speeds up the separation of photoexcited electrons.

The matched energy band of g-C_3N_4 and TiO_2 has been fruitful to couple them for constructing the heterojunction, which is considered an alternative to obtain maximized photocatalytic performance in comparison to individuals.[31,32] Therefore, TiO_2/g-C_3N_4 composite have been extensively researched in recent years, and most published works have shown that the coupling of g-C_3N_4 with TiO_2 is of greater importance benefiting from both g-C_3N_4 and TiO_2 properties.[31–36] Although the majority of these studies concentrate on the treatment of volatile chemical compounds, phenols, and organic pigments. There are very few studies related to the decomposition of organochlorine compounds, including 2,4-D, on TiO_2/g-C_3N_4 composite materials.

TiO_2 nanoparticles, like conventional TiO_2 powder, frequently have low specific surface areas, which could lead to poor photocatalytic performance. Consequently surface modification is a useful strategy for improving the photoresponse of TiO_2. By altering its surface structure, the adsorption ability of the catalyst may be enhanced and produce an increased number of radicals upon reaction with the photogenerated holes, both of which are advantageous for the photocatalytic activity.[37] TiO_2 nanotubes from nanoparticles has been synthesized via alkaline hydrothermal treatment. This method was firstly reported by Kasuga et al..[38] Due to the high surface area of the products produced after Kasuga, the hydrothermal approach of obtaining TiO_2-derived nanotubes has attracted special attention.[39–41]

In general, g-C_3N_4 is synthesized by the thermal condensation of reactive nitrogen-rich and oxygen free compounds typically including cyanamide, dicyanamide, triazine and heptazine derivatives. Although nitrogen-rich and oxygen-containing urea as a precursor gave rise to g-C_3N_4, the product yield was very low (only 4%).[42] Melamine has a honey-comb atomic arrangement which is very close to the expected one for g-C_3N_4. In addition, melamine structure has a relatively high nitrogen content of approximately 66.6% by mass of carbon nitride. Therefore melamine is the most commonly used s-triazine rings molecular precursor for the synthesis of graphitic g-C_3N_4.[43]

In this work, a modified TiO_2 with high surface area was synthesized by alkaline hydrothermal technique utilizing TiO_2 Degussa P25 as raw material. Several characterization techniques, including XRD, BET, SEM, UV-Vis DRS and photoluminescence (PL) were used to determine the impacts of alkaline hydrothermal treatment on the morphological, structural and photocatalytic properties of Degussa P25. The modified Degussa P25, also known as mod.TiO_2, was then combined with g-C_3N_4 to prepare mod.TiO_2/g-C_3N_4 composite. This was done in order to examine the impact of heterojunction structure on the photocatalytic performance of mod.TiO_2/g-C_3N_4 composite in the degradation of 2,4-D. The precursor for synthesis of g- C_3N_4 was melamine. The influence of pH and initial concentration of 2,4-D on the degradation efficiency was studied.

Experiment

Chemicals

Titanium dioxide Degussa P25 (Degussa P25) and melamine (99.0%) used for the preparation of photocatalysts were purchased from Sigma-Aldrich. Sodium hydroxide (NaOH) pellets (China) were used to modify TiO_2 P25 to obtain mod.TiO_2. All chemicals were used without further purification.

Materials Synthesis

Preparation of Mod.TiO_2

Degussa P25 powder was altered via an alkaline hydrothermal process as reported by Kasuga et al[38] in order to enhance the porous surface. The procedure is as follows: 2.0 g of Degussa P25 was submerged in 50 mL of a 10 M NaOH solution for 20 minutes. The combination was then hydrothermally heated for 12 hours at 150 °C. After rinsing the product in water to lower its pH, it was immersed in a 0.1 M HCl solution for two hours. The product was then washed with distilled water until the pH reached 7, dried at 80 °C overnight, and then heated at 400 °C for two hours. The alkaline treated Degussa P25 is denoted as mod.TiO_2.

Preparation of Pristine G-C_3N_4

Pristine g-C_3N_4 was prepared through the thermal decomposition of melamine.[44] Briefly, 10 g of melamine is finely ground on an agate mortar, then the sample was heated at 520 °C for 4 hours in a muffle furnace with a heating rate of 5 °C/min. After cooling to room temperature, the sample was rinsed multiple times with distilled water and then washed with absolute ethanol. Finally, the product was dried at 80 °C overnight and stored in sealed containers.

Preparation of Mod.TiO_2/G-C_3N_4

Mod.TiO_2 and melamine were mixed and ground in an agate mortar. Then, they were heated in a muffle furnace at 520 °C for 4 hours with a heating rate of 5 °C/min. After cooling to room temperature, the sample was rinsed multiple times with distilled water and then washed with absolute ethanol. Finally, the product was dried at 80 °C overnight and stored in sealed containers. The two samples were synthesized with 30% and 50% by weight of mod.TiO_2. The synthesized samples are denoted as 30% mod.TiO_2/g-C_3N_4 and 50% mod.TiO_2/g-C_3N_4.

Characterization Techniques

The energy dispersive X-ray spectroscopy (EDX) to determine elemental composition, and SEM images to evaluate the morphology of the material were performed on the FESEM S-4800 equipment system. The ultraviolet-visible diffuse reflectance spectrum (UV-Vis DRS spectrum) to evaluate the light absorption ability of the materials was performed on a Shimadzu UV-2600 device. The

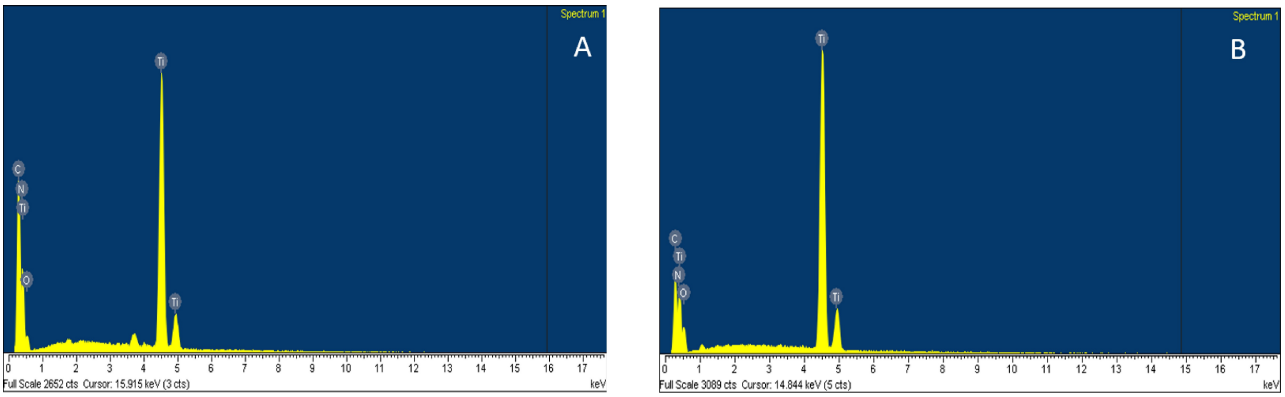

Figure 1. EDX spectra of (A) 30% mod.TiO_2/g-C_3N_4 and (B) 50% mod.TiO_2/g-C_3N_4.

photoluminescence spectroscopy (PL spectrum) to estimate the recombination rate of photogenerated electron–hole pairs was carried out on the FLS1000 Photoluminescence Spectrometer. The N_2 adsorption-desorption method at 77 K to determine the textile properties was measured on TriStar 3000V6 07A equipment; The X-ray diffraction (XRD) spectroscopy to evaluate the presence of crystalline phases was carried out on a Bruker D8 Advance diffraction machine with a Cu–K radiation source (wavelength 0.15418 nm).

Photocatalytic Activity Evaluation

The photocatalytic activity of synthesized catalysts was defined by the photodegradation of 2,4-D as the model pollutant. In a typically photocatalytic reaction 150 mL of 2,4-D solution with an initial concentration of 40 ppm, at a pH of 2.1, and 75 mg of the as-prepared catalyst mass (a mass-to-volume ratio of 0.5 g/L) were utilized in all experiments. The solution was constantly stirred by a magnetic stirrer and was irradiated with a 250 W compact xenon arc lamp (Model No. CHF XM500 W with a UV cut-off filter ($\lambda >$ 400 nm)) which was fixed 20 cm above the solution surface. The reaction system was a quartz glass beaker placed on a thermostatic surface to maintain a constant temperature of 25 °C. At regular time intervals (30 minutes) 3 mL of solution were withdrawn and analyzed using a UV-vis spectrophotometer at a wavelength of 283 nm. Reaction conditions are always maintained constant in this study, unless specified otherwise.

The percentage 2,4-D removal efficiency was calculated using the formula:

$$2,4-D\ removal\ efficiency\ (H\%) = \frac{(C_0 - C_t)}{C_0} \times 100\,\% \qquad (1)$$

where C_o is the 2,4-D initial concentration and C_t is the 2,4-D concentration obtained after various intervals of time t.

Results and Discussion

Characterization of As-Synthesized Materials

Energy Scattering Spectroscopy (EDX)

EDX spectra were measured for two samples: 30% mod.TiO_2/g-C_3N_4 and 50% mod.TiO_2/g-C_3N_4 (estimated according to the reaction equation). The results are presented in Figure 1 and Table 1.

In two samples, the calculated mass percentages of mod.TiO_2 are 28.5% and 52.0%, respectively, which closely match the predicted quantities. This strong concordance may be considered as proof that the synthesis process worked. Furthermore, the sample can be regarded as extremely pure because it solely comprises the components C, N, and Ti. According to EDX spectra, the weight percentages of mod.TiO_2 in the samples do not differ substantially from the predicted values. Therefore, in further studies, the designations of 30% and 50% mod.TiO_2/g-C_3N_4 will be kept for convenience.

FESEM Analysis

The morphological structures of Degussa P25, mod.TiO_2, and mod.TiO_2 /g-C_3N_4 composites were explored by FESEM, and the results are displayed in Figure 2 and Figure 3.

It can be observed that Degussa P25 (Figure 2A) has a particle-like structure, fairly uniform in size with an average particle size of approximately 30 nm. Following modification, there is a dramatic shift in the surface morphology, changing from a spherical structure to a fibrous, tubular one. With an average length of several micrometers and a width of roughly 100–200 nm. The surface becomes more porous and uniformly

Table 1. Chemical elemental compositions from EDX spectra (wt%).

Samples	C	N	O	Ti	Total (%)	The actual %TiO_2
30% mod.TiO_2/g-C_3N_4	26.81	40.54	9.13	23.52	100.00	28.5
50% mod.TiO_2/g-C_3N_4	18.14	27.41	20.73	33.72	100.00	52.0

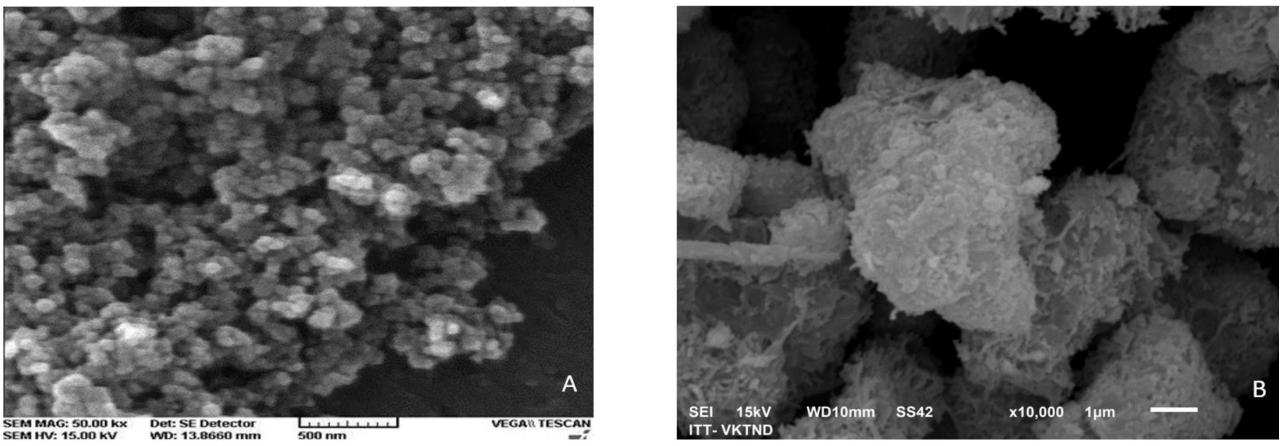

Figure 2. FESEM images of (A) Degussa P25; and (B) mod.TiO_2.

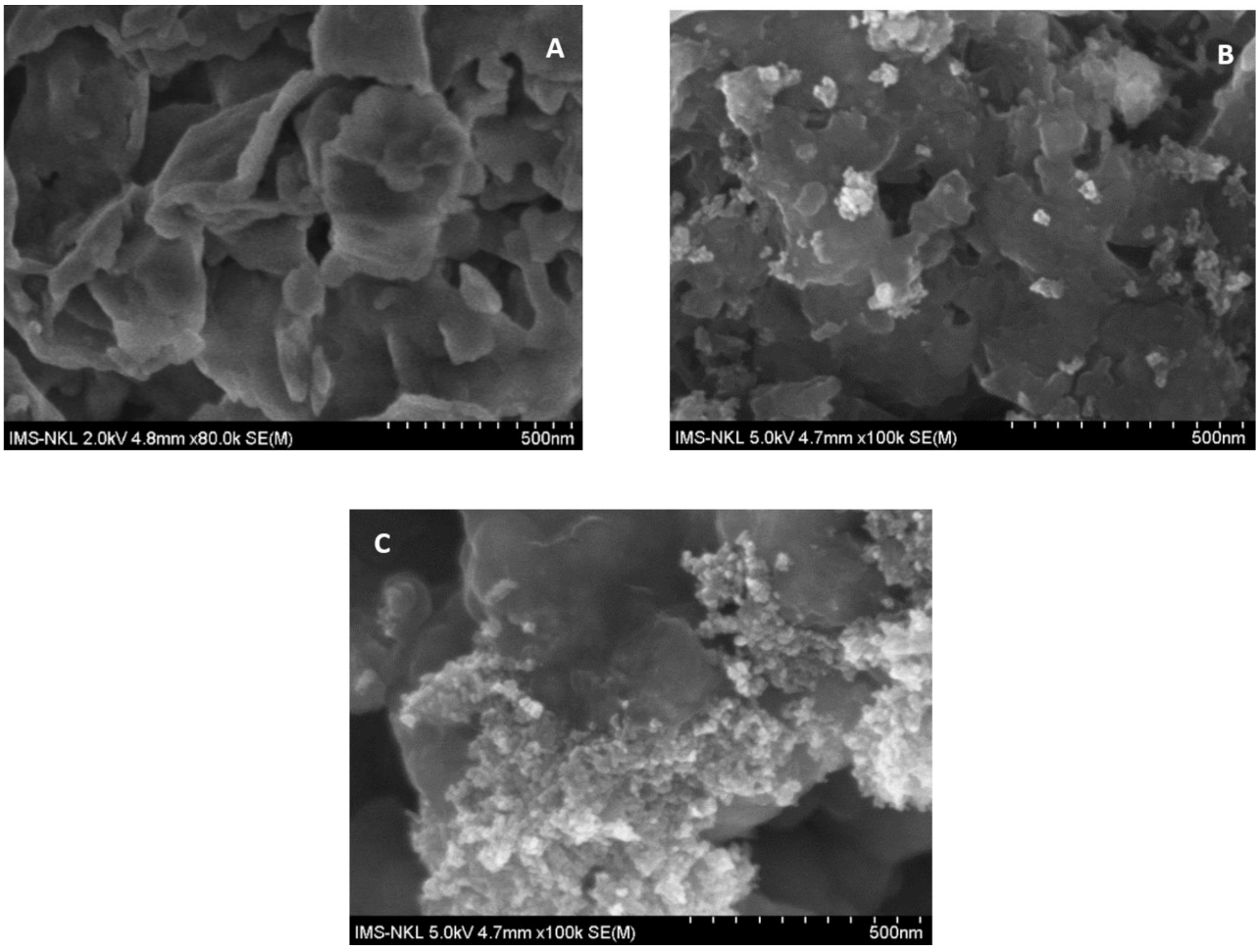

Figure 3. FESEM images of (A) pristine g-C_3N_4; (B) 30 % mod.TiO_2/g-C_3N_4; and (C) 50 % mod.TiO_2/g-C_3N_4.

distributed (Figure 2B). The lack of spherical particles (bulk form) in the FESEM image of mod.TiO_2 suggests a porous structure with tiny fibers, which gives TiO_2 a high specific surface area that can be obtained using the hydrothermal technique in NaOH.

As evident from Figure 3A, pristine g-C_3N_4 has a transparent 2D nanosheet-like structure with ultrathin thickness. In the case of composites, Figure 3B and 3 C show that mod.TiO_2 was embedded in the g-C_3N_4 structure, aggregated into small clusters. As the mod.TiO_2 content increases, these small clusters also gradually enlarge, and the components appear to be closer

to each other. These suggest the formation of a heterojunction among mod.TiO_2 and g-C_3N_4 which might improve electron–hole separation and photocatalytic activity. Moreover, in all cases a porous structure can be observed, as was indicated by the results of nitrogen physisorption analysis.

X-Ray Diffraction Spectroscopy (XRD) Analysis

The crystallographic structure of synthesized photocatalysts was examined using XRD and experimental data are displayed in Figure 4.

In Figure 4A we can observe that the XRD patterns of both Degussa P25 and mod.TiO_2 show the representative characteristic peaks of phases (101), (004), (200), (105), (211), and (204) at 2θ of 25.33°, 37.82°, 48.06°, 53.93°, 55.05°, and 62.63°, respectively. This result is consistent with standard data for the anatase phase (JCPDS Card No. 21–1272). It is worth noting that the XRD pattern of mod.TiO_2 exhibits high-intensity and sharp peaks, indicating that the alkaline hydrothermal treatment does not reduce the crystallinity of Degussa P25 precursor.

The pristine g-C_3N_4 (Figure 4B) exhibits a single characteristic diffraction peak located at 2-θ position 27.5°, which corresponds to the (002) plane of the interlayer stacking of conjugated aromatic system of g-C_3N_4 (JCPDS Card No. 87–1526).[29, 30] diffraction peaks of mod.TiO_2 and pristine g-C_3N_4 are visible in the XRD patterns for the mod.TiO_2/g-C_3N_4 nanocomposites, indicating the coexistence of these compounds in the composites. However a slight change in the nanocomposites was noticed: when the amount of mod.TiO_2 in the composite decreases, the intensity of the characteristic peaks for mod.TiO_2 gradually weakens, while the peaks specific to g-C_3N_4 gradually intensify, indicating a strong interaction between g-C_3N_4 and mod.TiO_2. Our finding is in agreement with the work done by M. Roškarič, G. Žerjav, M. Finšgar et al.[45] where g-C_3N_4/TiO_2 photocatalyst was investigated. The authors speculated that this phenomenon was observed due to the favorable electronic properties of two components, which can interact when the heterojunction is formed.

UV-Visible Diffuse Reflectance Spectroscopy (UV-Vis DRS) Analysis

The UV-vis DR measurements were performed to determine the light absorption properties of the synthesized materials.

Figure 5 illustrates the UV-Vis diffuse reflectance spectra of Degussa P25, mod.TiO_2, g-C_3N_4, 30% mod.TiO_2 /g-C_3N_4, and 50% mod.TiO_2/g-C_3N_4 recorded in the UV and Vis regions (wavelengths from 250 to 800 nm).

As shown in Figure 5A, Degussa P25 exhibits strong ultraviolet (UV) light absorption with an absorption edge at 360 nm. In comparison to the pristine one the optical absorption of mod.TiO_2 undergoes negligible changes, with the intensity and position of the absorption peak remaining at around 360 nm. However, a slight red shift of the absorption peak can be observed. Pristine g-C_3N_4 shows intensive light absorption capability in both ultraviolet and visible light regions with an absorption edge at around 430 nm (Figure 5B). Whereas, upon coupling mod.TiO_2 with g-C_3N_4, the composite exhibits an significant improvement in visible light absorption owing to the strong and wide absorption band of g-C_3N_4 in the visible region. The absorption edge of the composites shows a red shift as compared to mod.TiO_2, which can be attributed to the interaction between g-C_3N_4 and TiO_2. The enhancement of light absorption of the nanocomposite in both ultraviolet and visible regions is crucial for photocatalytic activity under solar light irradiation.

Further, the energy band gap (E_g) values of investigated samples were estimated using the Kubelka-Munk theory (Eq. (2)):[46]

$$(\alpha.h\upsilon)^n = A(h\upsilon - Eg) \quad (2)$$

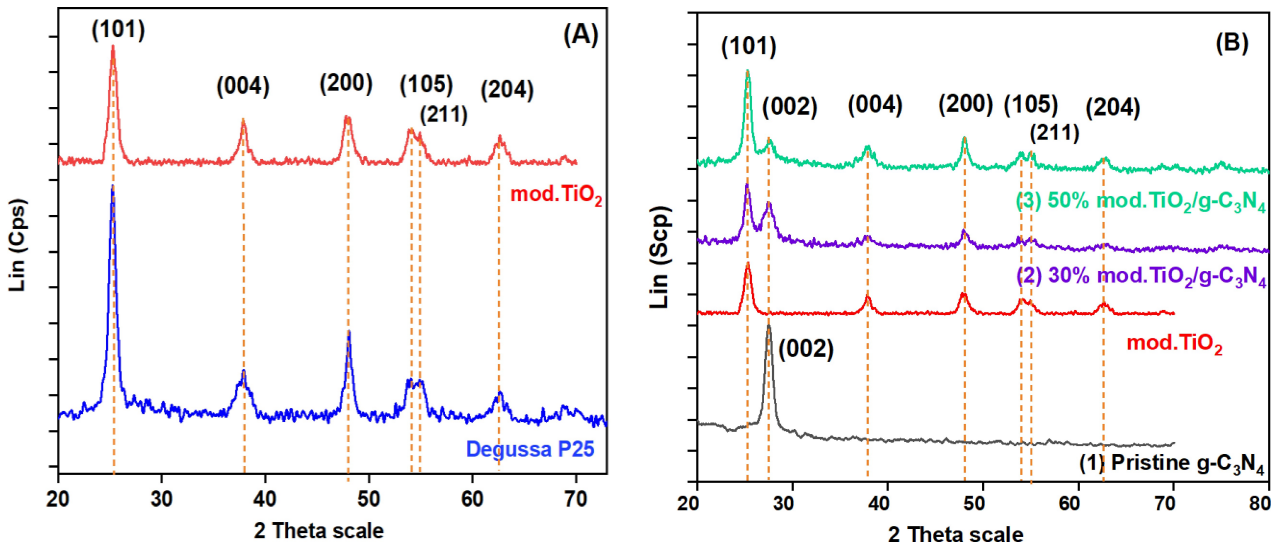

Figure 4. (A) X-ray diffraction spectra of (A) Degussa P25, mod.TiO_2; and (B) g-C_3N_4, 30% mod.TiO_2/g-C_3N_4, and 50% mod. TiO_2/g-C_3N_4.

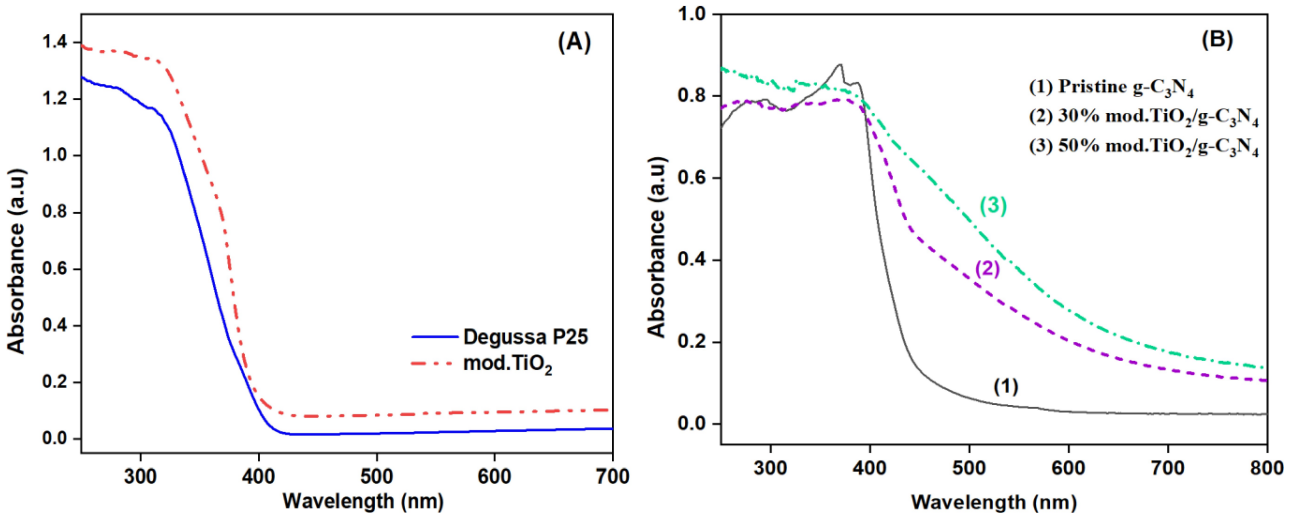

Figure 5. UV-Vis DRS of (A) Degussa P25 and mod.TiO_2; (B) g-C_3N_4, 30% mod.TiO_2/g-C_3N_4, and 50% mod.TiO_2/g-C_3N_4.

Where α is the optical absorption intensity (a.u), h is the Planck's constant ($h = 6.625 \times 10^{-34}$ Js), ν is the frequency of the incident radiation ($\nu = c/\lambda$, where c is the speed of light and λ is the wavelength), $n = 1/2$ and A is a proportionality constant.

The estimated energy band gaps for synthesized samples are listed in Table 2.

From Table 2 it can see that the band gap of Degussa P25 is 3.1 eV, and this value decreases to 2.9 eV when Degussa P25 undergoes alkaline hydrothermal treatment. Notably, the reduction in the band gap of mod.TiO_2 is achieved without doping metallic or non-metallic. The further reduction in the band gap when mod.TiO_2 is coupled with g-C_3N_4 (Figure 6B and Table 2) is attributed to the incorporation of g-C_3N_4, promoting the generation of more charge carriers in the composite material under visible light irradiation. The experimental data obtained align well with our previous theoretical calculations[47] and the work conducted by N. Madima et al..[34]

Photoluminescence (PL) Analysis

The photoluminescence (PL) emission spectra have been used to assess the recombination rate of charge carriers in the photocatalysts. A higher emission intensity in the PL spectrum

Table 2. The energy band gaps of Degussa P25, mod.TiO_2, g-C_3N_4, 30% mod.TiO_2 /g-C_3N_4 and 50% mod.TiO_2/g-C_3N_4.

Samples	Degusa P25	Mod.TiO_2	g-C_3N_4	30% mod.TiO_2 /gC_3N_4	50% mod.TiO_2/g-C_3N_4
E_g (eV)	3.1	2.9	2.7	2.3	1.7

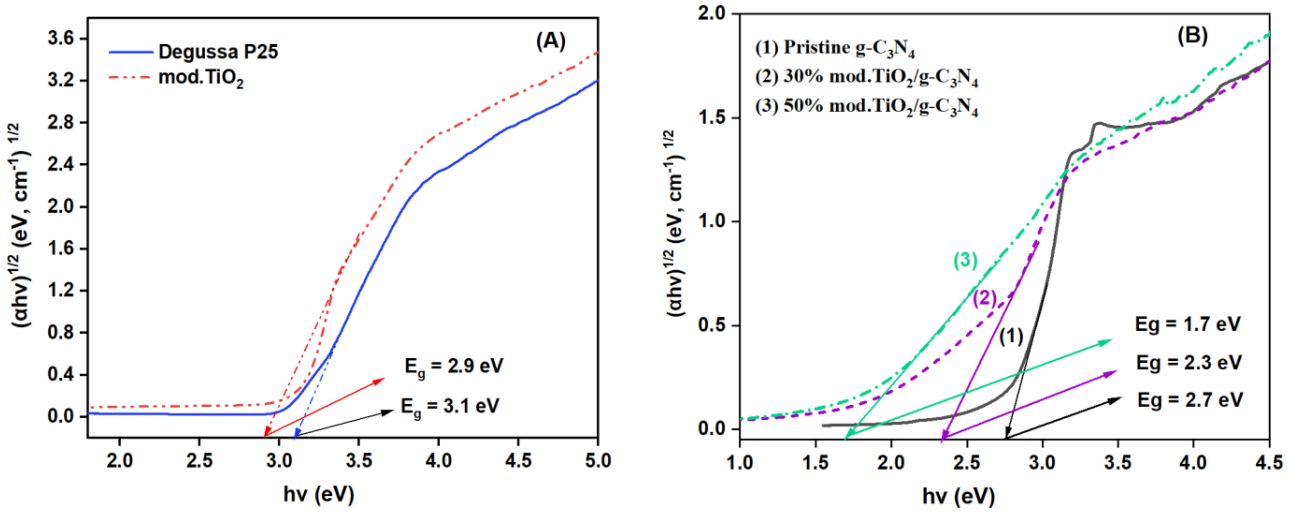

Figure 6. The plot $(\alpha.h\upsilon)^{1/2}$ vs $(h\upsilon)$ of (A) Degussa P25 and mod.TiO_2; and (B) g-C_3N_4 , 30% mod.TiO_2/g-C_3N_4, and 50% mod.TiO_2/g-C_3N_4.

indicates a higher probability of recombination. From Figure 7A it can be observed that the modified and unmodified Degussa P25 exhibit quite similar PL emission bands. Figure 7B displays the PL emission spectra of pristine g-C_3N_4 and mod.TiO_2/g-C_3N_4 composites. The PL spectrum of g-C_3N_4 reveals a strong photoluminescence signal, demonstrating a high recombination rate of electron–hole pairs. The PL spectra of mod.TiO_2/g-C_3N_4 composites show a lower photoluminescence signal indicating a low recombination rate of electron–hole pair. The PL intensity decreases in the order of pristine g-C_3N_4 > 30% mod.TiO_2/g-C_3N_4 > 50% mod.TiO_2/g-C_3N_4. Therefore, the combination between mod.TiO_2 and g-C_3N_4 is favorable as it can reduce the charge carrier recombination tendency, especially for the 50% mod.TiO_2/g-C_3N_4 sample. Our result is consistent with the finding of M. Roškarič, G. Žerjav, M. Finšgar et al.[45] and R. Hao et al..[48]

BET Analysis

Nitrogen adsorption-desorption at 77 K was carried out to determine the textural properties of synthesized photocatalysts and the results are shown in Figure 8.

Table 3 demonstrates the measured surface areas (S_{BET}), total pore volumes (V_{tot}), and average pore diameters (D) of the synthesized photocatalysts.

From Figure 8 it can see that all synthesized photocatalysts resemble type IV isotherms according to the IUPAC description,[49] which implies that all samples possess mesoporous structures. The results in Table 3 show that Degussa P25 is a mesoporous material with a relatively low specific surface area (56.31 $m^2 g^{-1}$) and a total pore volume between particles of 0.3406 $cm^2 g^{-1}$. The alkaline hydrothermal treatment induces a significant improvement in its porous characteristics: the specific surface area reaches 123.52 $m^2 g^{-1}$ with a total pore volume of 0.6923 $cm^3 g^{-1}$. Upon coupling to g-C_3N_4, the surface

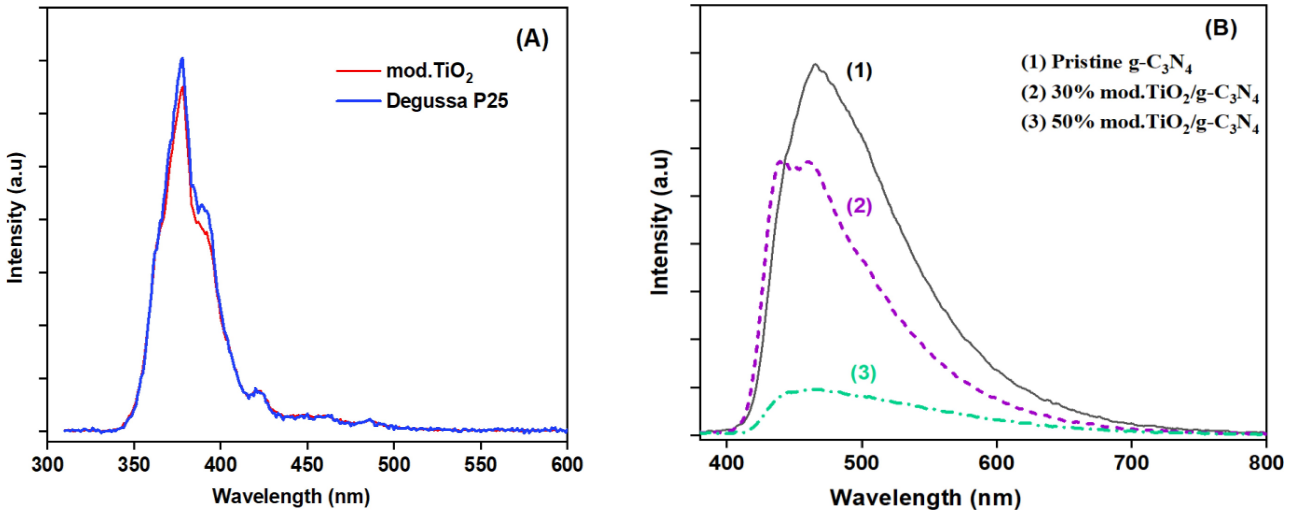

Figure 7. PL spectra of (A) Degusa P25 and mod.TiO_2; and (B) g-C_3N_4 , 30% mod.TiO_2 /g-C_3N_4, and 50% mod. TiO_2/g-C_3N_4.

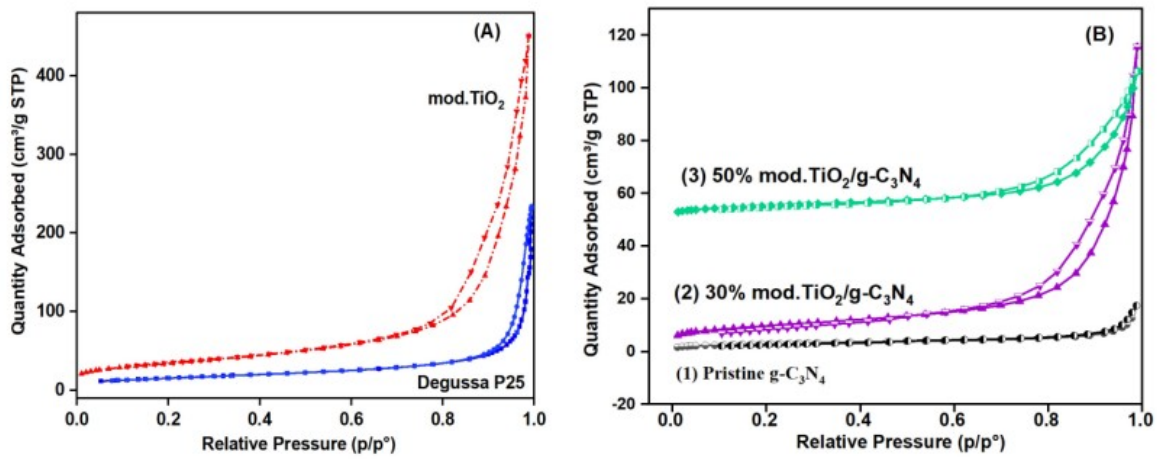

Figure 8. The N_2 adsorption-desorption diagram at 77 K of (A) Degussa P25 and mod.TiO_2 ; and (B) g-C_3N_4, 30% mod.TiO_2/g-C_3N_4, and 50% mod.TiO_2/g-C_3N_4.

Table 3. Specific surface area, total porous volume, and average pore diameter.

Samples	S_{BET} (m^2g^{-1})	V_{tot} (cm^3g^{-1})	D (nm)
Degussa P25	56.3	0.3406	26.20
Mod.TiO_2	123.5	0.6923	29.22
Pristine g-C_3N_4	10.7	0.2473	16.32
30% mod.TiO_2/g-C_3N_4	34.7	0.1624	24.60
50% mod.TiO_2/g-C_3N_4	19.2	0.0822	20.07

area of mod.TiO_2 decreases, from 123.52 m^2g^{-1} down to 34.66 m^2g^{-1} for 30% mod.TiO_2/g-C_3N_4 and 19.19 m^2g^{-1} for 50% mod.TiO_2/g-C_3N_4. The reason for the lower average pore volumes of mod.TiO_2 /g-C_3N_4 composites (0.124 cm^3g^{-1} and 0.0822 cm^3g^{-1}) compared to mod.TiO_2 (0.6923 cm^3g^{-1}) could be the result of pore blockages cause by the combination of mod.TiO_2 and g-C_3N_4.[34] On the other hand, the mod.TiO_2/g-C_3N_4 composites were shown to have a higher specific surface area than g-C_3N_4: pure g-C_3N_4 has a characteristic low specific surface area of 10.72 m^2g^{-1}, the addition of mod.TiO_2 increases the specific surface area. A higher surface area increases the adsorption capability due to the existence of more active sites, while a larger pore structure permits for more 2,4-D to be adsorbed on the surface of the photocatalysts.

The Advantages of Alkaline Hydrothermal Treatment

The influence of the alkaline hydrothermal treatment on photocatalytic activity of TiO_2 was determined by conducting concurrently the degradation of 2,4-D under UV light for both untreated Degussa P25 and treated Degussa P25. Experimental conditions were: initial concentration of 2,4-D = 0.069 gL^{-1}, catalyst mass = 25 mg, 2,4-D solution volume = 50 mL, stirring time in the dark = 30 minutes, total irradiation time = 150 minutes. The results are presented in Figure 9. As depicted in Figure 9, Degussa P25 exhibited no 2,4-D adsorption, whereas mod.TiO_2 had a moderate adsorption capacity for 2,4-D. This may be explained by the alkalinization of Degussa P25, which increased the surface area (from 56 m^2g^{-1} for Degussa P25 to 123 m^2g^{-1} for mod.TiO_2, Table 3) and made the TiO_2 surface more porous. Additionally, it was shown that when exposed to UV radiation, mod.TiO_2 exhibited a greater 2,4-D photocatalytic degradation efficiency when compared to untreated Degussa P25. This indicates that specific surface area and band gap have a major influence on 2,4-D photocatalytic degradation.

The results regarding the changes in photocatalytic activity directly reflect differences in the light absorption capability as well as the electron–hole recombination ability of untreated Degussa P25 and mod.TiO_2, as indicated in the UV-Vis DRS results and PL spectra.

Adsorption Test

The adsorption study were carried out for pristine g-C_3N_4 and for 30%mod.TiO_2/g-C_3N_4 composite, and the results reveal that only 1% and 7% removal efficiency were obtained after 240 min over g-C_3N_4 and 30%mod.TiO_2/g-C_3N_4, respectively. The obtained results are presented in Figure 10. Based on these results, further experiments assessing catalytic activity in the photodegradation of 2,4-D were conducted under the conditions outlined in the experimental section. The photocatalytic performance of the synthesized samples was observed by monitoring the main absorption peak of 2,4-D at 283 nm.

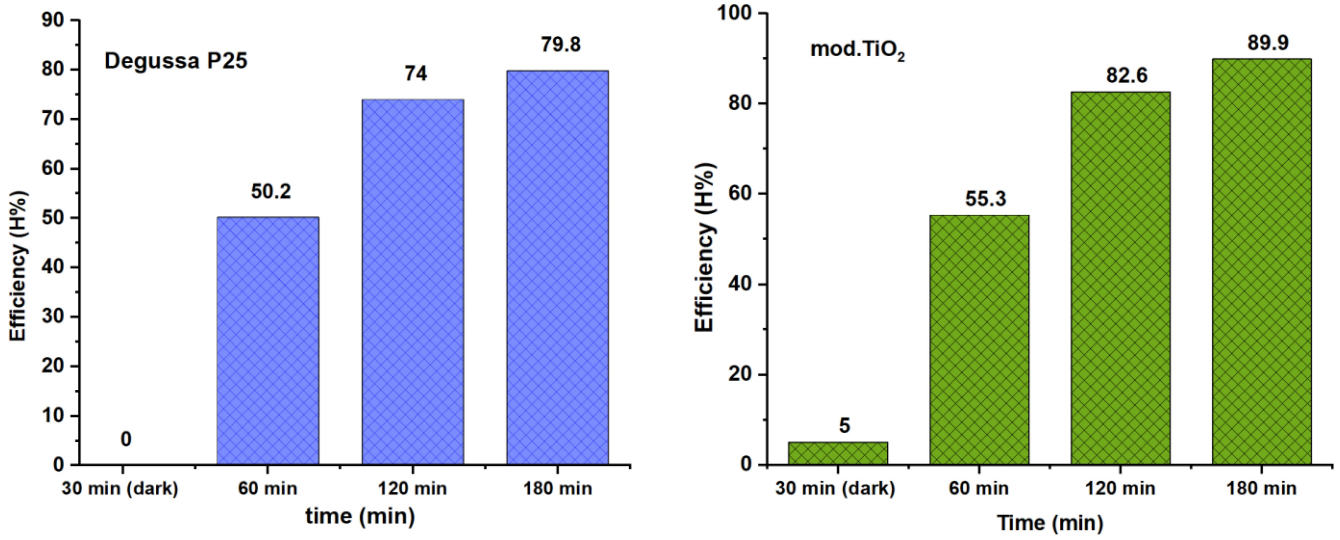

Figure 9. The photocatalytic activity of Degussa P25 and mod.TiO_2 in the 2,4-D degradation.

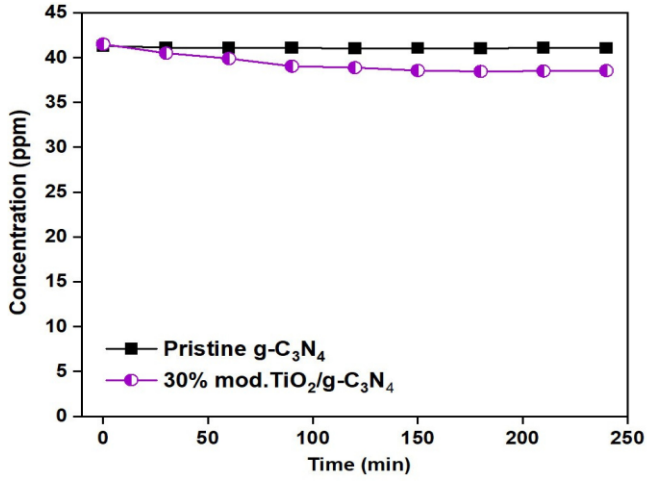

Figure 10. The 2,4-D concentration vs. adsorption time over prisstine g-C_3N_4, and 30%mod.TiO_2/g-C_3N_4 (C_o = 40 ppm, pH = 2.1, 240 min adsorption).

Evaluation of 2,4-D Degradation Efficiency of Mod.TiO_2/G-C_3N_4

Influence of Mod.TiO_2 Loading

The photodegradation of 2,4-D over mod.TiO_2, pristine g-C_3N_4, 30%mod.TiO_2/g-C_3N_4, and 50%mod.TiO_2/g-C_3N_4 were carried out. The obtained results are presented in Figure 11.

The experimental results show that the investigated composites exhibit higher 2,4-D degradation activity than individuals. These results further show that only minor 2,4-D adsorption onto the catalyst surface occurred. In the first 60 minutes of illumination, the decrease in 2,4-D concentration is not significant and H% were 23.5%, 14.0%, 4.98%, and 0.07% for 50%mod.TiO_2/g-C_3N_4, 30%mod.TiO_2/g-C_3N_4, mod.TiO_2, and g-C_3N_4, respectively. This could be attributed to the weak adsorption of 2,4-D by both g-C_3N_4 and mod.TiO_2. The lack of synergistic adsorption-catalysis effects leads to a slow initial reaction time.

After 210 minutes of illumination, the 2,4-D degradation efficiency of 80.65%, 70.68%, 83.56%, and 86.95% were achieved over mod.TiO_2, pristine g-C_3N_4, 30%mod.TiO_2/g-C_3N_4 and 50%mod.TiO_2/g-C_3N_4, respectively.

The improved photocatalytic activity of the composites can be attributed to the decrease in the photogenerated electron-hole recombination due to the development of the hetero-junction structure. The highest 2,4-D degradation observed over 50%mod.TiO_2/g-C_3N_4 can be credited to the improved contact between the components, which results in the improvement of the charge carrier separation and the better utilization of the charge carriers for the formation of ROS.

Influence of 2,4-D initial Concentration

Four experiments were conducted concurrently over 50% mod.TiO_2/g-C_3N_4 catalyst and the results are presented in Figure 12.

From Figure 12, it can be seen that when the 2,4-D initial concentration increases from 25 ppm to 40 ppm, the degradation efficiency decreases slightly from 97.33% to 86.95%. A further increase in the 2,4-D concentration results in a drastic decline of photocatalytic performance. Therefore, the highest photodegradation efficiency of 2,4-D was obtained to be 97.33% over 50% mod.TiO_2/g-C_3N_4 catalyst at an initial 2,4-D concentration of 25 ppm. At higher concentration, a large proportion of 2,4-D are adsorbed on the catalyst surface, which hinders the light penetration, reduces the active sites for the generation of ROS, and results in a decrease in the 2,4-D degradation. Similar trends have been reported by other researchers for catalytic degradation of the other contaminant.[3, 5, 50]

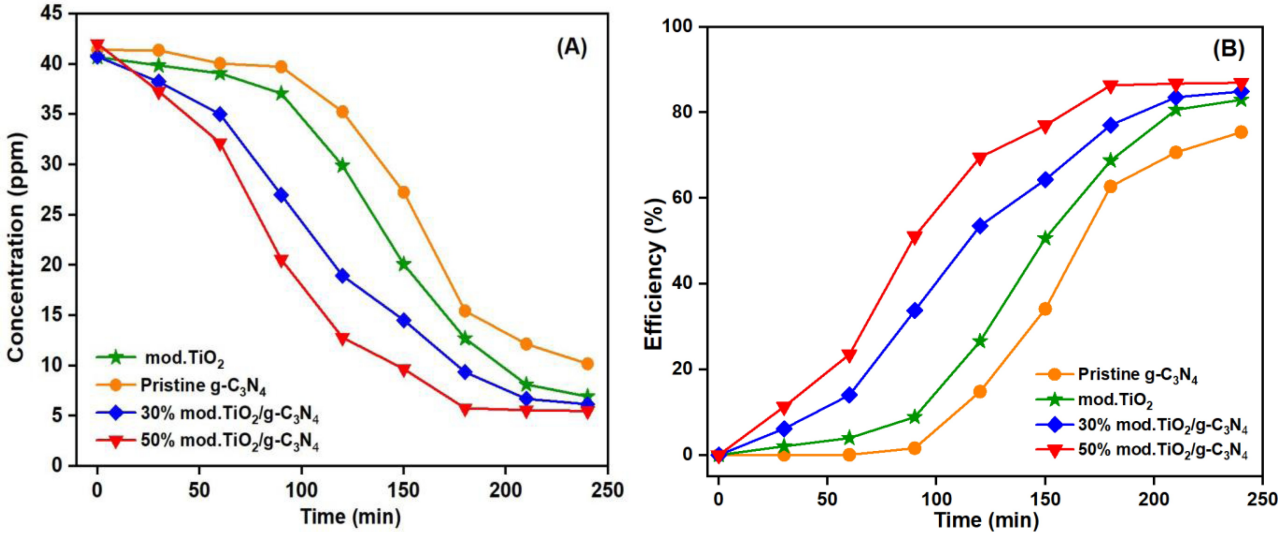

Figure 11. (A) The 2,4-D concentration, and (B) The degradation efficiency vs. illumination time over g-C_3N_4, mod.TiO_2, 30%mod.TiO_2/g-C_3N_4 , and 50% mod.TiO_2/g-C_3N_4 (C_o = 40 ppm, pH = 2.1, 240 min illumination).

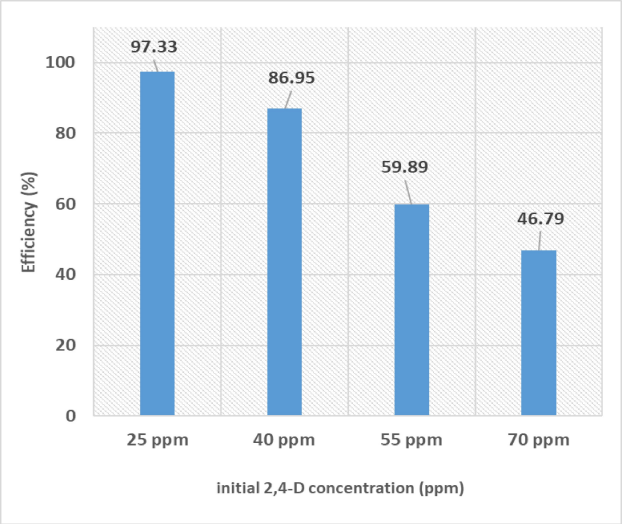

Figure 12. The photocatalytic efficiency, *H%*, as a function of 2,4-D initial concentration, C_o (pH = 2.1, 210 min illumination).

Influence of PH

Three photocatalytic degradation experiments of 2,4-D over 50% mod.TiO_2/g-C_3N_4 were carried out at three different pH levels, namely 2.1, 5.0, and 8.0. The results are shown in Figure 13.

As indicated in Figure 13, the degradation efficiency of 2,4-D decreases with an increase in pH level. Specifically, after 210 min illumination, the degradation efficiency of 2,4-D was 86.95% at pH 2.1, but it decreased to 60.01% and 50.09% at pH 5.0 and pH 8.0, respectively. The result indicates that the photocatalytic degradation of 2,4-D is favorable at low pH. The highest degradation efficiency of 2,4-D was achieved at pH 2.1. This can be explained based on the formation of free radicals in the photocatalytic activity mechanism of the semiconductor material.[51]

Radical Scavengers Test

To work out which reactive oxygen species (ROS) play a major role in the photodegradation process of 2,4-D over the mod.50%TiO_2/g-C_3N_4 nanocomposite, several quenching experiments were conducted. Two quenchers: ISP and 0.01 M Na-EDTA were employed to trap the hydroxyl radical (•OH), and hole (h^+), respectively, and the results are displayed in Figure 14.

The 2,4-D degradation efficiency was significantly reduced when radical scavengers were introduced. Specifically, the degradation efficiency of 2,4-D decreases from 86.95% to 11.53% as EDTA was added to the reaction mixture, and to 10.08% when using an •OH radical scavenger (supplemented with isopropanol). Therefore, both •OH radical and h^+ play an important role in the degradation process of 2,4-D over mod.TiO_2/g-C_3N_4 materials under visible-light illumination.

Proposed Mechanism of the Photoexcitation and Photodegradation of 2,4-D

From the UV-Vis DRS measurements, the CB and VB potentials of mod.TiO_2 and g-C_3N_4 were estimated using equations (3) and (4)[45,48]

$$E_{VB} = \chi - E^e + 0.5E_g \quad (3)$$

$$E_{CB} = E_{VB}\text{-}E_g \quad (4)$$

Where χ is the electronegativity (~4.73 eV for g-C_3N_4 and ~5.81 eV for TiO_2); E^e is the energy of free electrons on the hydrogen scale (~4.5 eV); E_g is the energy bandgap. The

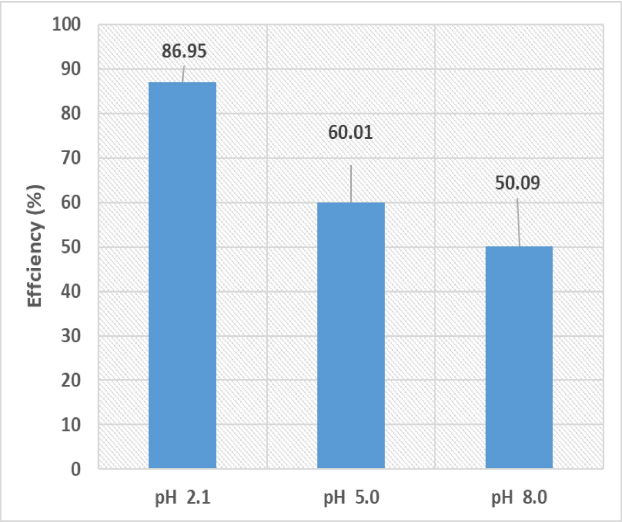

Figure 13. The efficiency of 2,4-D photodegradation over 50%mod.TiO_2/g-C_3N_4 at different pH (C_o = 40 ppm; 210 min illumination).

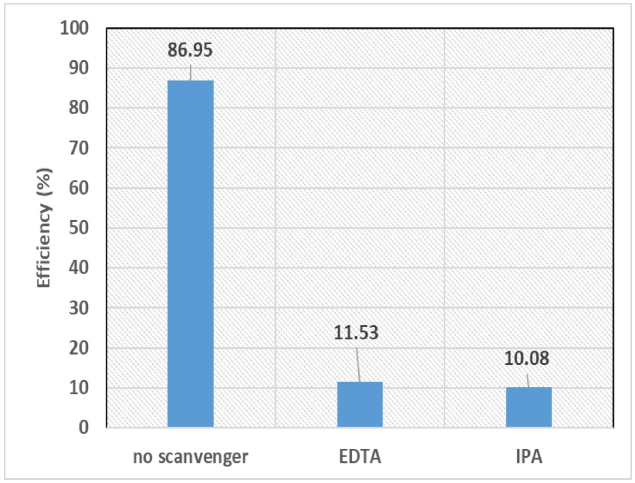

Figure 14. The degradation efficiency of 2,4-D in the cases of adding 0.01 M Na-EDTA, isopropanol (99%), and without radical scavengers (C_o = 40 ppm; pH = 2.1, 210 min illumination).

estimated VB and CB potentials for g-C_3N_4 and mod.TiO_2 are 1,58 eV and −1,12 eV, 2,76 eV and −0.14 eV respectively.

From the literature[45,48,52–55] and the calculated values of CB and VB potentials a generation of photoinduced charge carrier and photocatalytic mechanism may be proposed as in Scheme 1 which is consistent with the aforementioned quenching experiment.

When stimulated with a suitable light source,[17,29,30] electrons in the valence band (VB) of g-C_3N_4 and mod.TiO_2 jump to the conduction bands (CB), resulting in a CB rich in electrons (e^-) and leaving behind in the VB holes (h^+). Due to E_{CB} of g-C_3N_4 (− 1.12 eV) is more negative than that of mod.TiO_2 (−0.14 eV) therefore, the generated electrons in the CB of g-C_3N_4 can transfer down to the CB of TiO_2, preventing these electrons (e^-) from recombining with the holes (h^+) in the VB of g-C_3N_4. This results in the efficient separation of photogenerated electrons and holes. The suggested behaviour is also

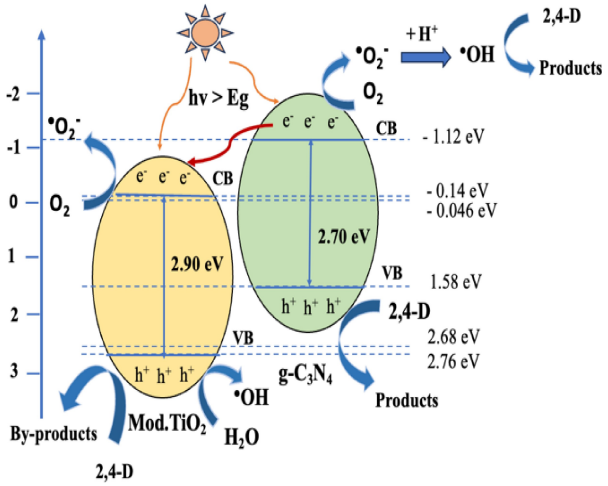

Scheme 1. The suggested photocatalytic mechanism for mod. TiO_2/g-C_3N_4 in acid media under visible-light illumination.

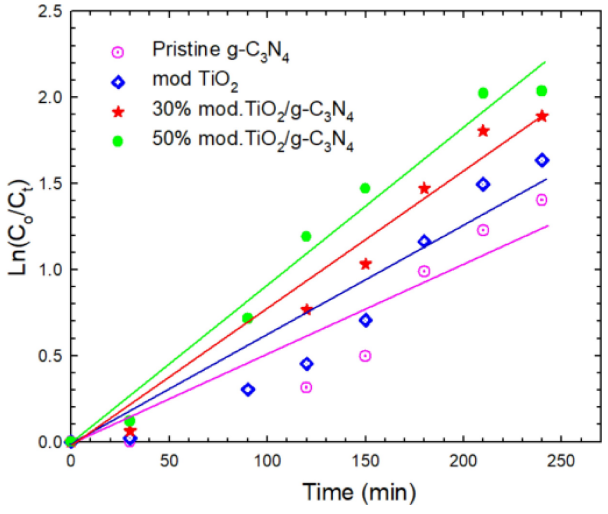

Figure 15. Apparent pseudo-first-order reaction kinetics for photocatalytic degradation of 2,4-D over synthesized materials (C_o = 40 ppm, pH = 2.1, 240 min irradiation). The symbols denote experimental data points. The solid lines are linear fits to appropriate time ranges.

supported by our previous theoretical results.[47] The conduction band of TiO_2 is electron-rich, and these electrons react with water-dissolved oxygen (the reduction potential of oxygen −0.046 eV vs. NHE) to generate superoxide radicals ($O_2^{\bullet-}$). In acid environment, $O_2^{\bullet-}$ continuously react forming •OH radicals.[26] On the other hand, the potential for the •OH/H_2O (2.68 eV vs.NHE) is too positive for the holes (h^+) in the VB of g-C_3N_4 to react with water to produce •OH radicals. Therefore the VB h^+ of g-C_3N_4 may directly react the 2,4-D. In addition, when •OH scavenger was added, the degradation of 2,4-D was slower. Thus a certain amount of hydroxyl radical may be produced in the catalytic process. Because E_{VB} of mod.TiO_2 (2.76 eV vs. NHE) is more positive than the potential of •OH/H_2O so the VB holes of mod.TiO_2 can oxidize water (H_2O) to generate hydroxyl radicals (•OH). Therefore, $O_2^{\bullet-}$, •OH, and h^+ are main ROS accountable for 2,4-D degradation under our experimental conditions. The experiments were conducted at pH value of 2.1 then the effect of pH value could be described as Eqs. (5) – (11):[56, 57] ffr11 >

$$\text{Mod.TiO}_2/\text{g-C}_3\text{N}_4 + h\nu \rightarrow \text{mod.TiO}_2/\text{gC}_3\text{N}_4\ (e^- + h^+) \quad (5)$$

$$e^- + O_2 \rightarrow {}^{\bullet}O_2^- \quad (6)$$

$${}^{\bullet}O_2^- + H^+ \rightarrow HO_2^{\bullet} \quad (7)$$

$$2HO_2^{\bullet} \rightarrow H_2O_2 + O_2 \quad (8)$$

$$H_2O_2 + e^- \rightarrow {}^{\bullet}OH + HO^- \quad (9)$$

$$H_2O_2 + h\nu \rightarrow 2{}^{\bullet}OH \quad (10)$$

The VB holes in mod.TiO_2 can degrade 2, 4-D into by products.This proposed mechanism leads to enhanced photocatalytic degradation of 2,4-D in the presence of the mod.TiO_2/g-C_3N_4 composite materials under suitable illumination conditions.

Kinetics Evaluation

Kinetic analyses from many publised work show that the photocatalytic degradation can be approximated using pseudo-first-order kinetics, according to the Langmuir – Hinshelwood model:[3,5,8,57–59]

$$r = -\frac{dC}{dt} = k\,\frac{K_a C}{1 + K_a C} \quad (12)$$

At low initial substrate concentration the equation can be simplified to an apparent first-order equation :[57,58]

$$r = -\frac{dC}{dt} \approx k \times K_a C = k_{ap} C \quad (13)$$

Taking the integral of Eq. (12) yields Eq.(13)

Table 4. Kinetic parameters of 2,4-D photocatalytic degradation of 2,4-D over synthesized materials.

Materials	g-C_3N_4	mod.TiO_2	30 % mod.TiO_2/g-C_3N_4	50 % mod.TiO_2/g-C_3N_4
$k_{ap}(min^{-1})$	0.0051	0.0061	0.0078	0.0091
R^2	0.8764	0.9001	0.9694	0.9788

$$ln\frac{C_0}{C_t} = k_{ap}t \quad (14)$$

Where, K_a is the adsorption constant; k is the rate constant; k_{ap} is the apparent first – order rate constant; C_o and C_t are the initial concentration and concentration at a certain time (t) of the substrate, respectively.

In the experimental conditions established, the photocatalytic degradation of 2,4-D over synthesized materials could be fitted by the pseudo-first order kinetic equation (13) and the rate constants are the slopes of the straight lines. However, as can be seen from the plots showing the dependence of $ln(C_o/C_t)$ vs. time(t) in Figure 15, photocatalytic degradation of 2,4-D strictly follows the first-order kinetic model only over 30 % and 50 % mod.TiO_2/g-C_3N_4 composites during the whole illumination period (240 min), which is supported by the linear form of ln (Co/C) = f(t). This observation aligns with the above talks about the slow initial degradation rate of 2,4-D due to its limited adsorption ability by g-C_3N_4 and mod. TiO_2. The rate then starts to rise gradually.

The kinetic parameters of the photocatalytic degradation of 2,4-D are presented on Table 4. The photocatalytic reaction rates of different materials increase in the following order: g-C_3N_4 < mod.TiO_2 < 30 % mod.TiO_2/g-C_3N_4 < 50 % mod.TiO_2/g-C_3N_4.

This order reflects the synergistic effects on the photogenerated charge transfer between the two semiconductor components, TiO_2 and g-C_3N_4. It also illustrates the significance of adsorption in heterogeneous catalysis, since poor adsorption will hinder the reaction kinetics. Mod.TiO_2 can adsorb 2,4-D thanks to its large surface area, which enhances the process of photocatalytic degradation.

Conclusions

In this work the effects of alkaline hydrothermal treatment and then further combination with g-C_3N_4 on the photocatalytic performance of a commercial TiO_2 catalyst (Degussa P25) in 2,4-D degradation were investigated.

A hydrothermal treatment of Degussa P25 particles at 150 °C under alkaline conditions leads to modified TiO_2 (mod.TiO_2) wire-like structure at NaOH concentration of 10 M. This is supported by measurement performed with analytical techniques: XRD, SEM, BET, UV-Vis DRS, and PL. Although the alkaline hydrothermal treatment increases the specific surface area and enhances the porous characteristics of mod.TiO_2, it does not significantly alter the energy band gap or the photoluminescence spectrum compared to pure Degussa P25. However the modification contributes remarkably to the enhancement of the photocatalytic activity, improving the adsorption of 2,4-D.

The 30 % and 50 %mod.TiO_2 /g-C_3N_4 materials were synthesized from mod.TiO_2 and g-C_3N_4 (with melamine as the precursor) using a combination of grinding and heating methods. The materials were characterized using EDX, XRD, SEM, BET, UV-Vis DRS, and PL techniques. The combination of mod.TiO_2 and g-C_3N_4 significantly enhances the light absorption properties of the mod.TiO_2/g-C_3N_4 composite materials compared to mod.TiO_2 and pristine g-C_3N_4. For photocatalytic activity, 30 % and 50 % mod.TiO_2/g-C_3N_4 show the highest photocatalytic activity due to the formation of the heterojunction structure of the composites. The decrease in the energy band gap of mod.TiO_2 upon coupling was attributed to the addition of the g-C_3N_4 phase, which stimulates the generation of more charge carriers in the nanocomposite under visible light radiation. The addition of ISP and EDTA results in a significant decrease in the photocatalytic activity of the nanocomposite, indicating that in the photodegradation experiments conducted under visible-light illumination in acid medium, both $^{\bullet}OH$, $^{\bullet}O_2^-$ free radicals and h^+ holes participate and play equivalent roles. The kinetic behavior was described in terms of the Langmuir–Hinshelwood model. The photocatalytic degradation of 2,4-D over synthesized materials seem follow pseudo-first order kinetics.

The results obtained in this study show that the simple hydrothermal treatment and then coupling to g-C_3N_4 may serve to boost the yields achieved by TiO_2 Degussa P25 in the photocatalytic degradation of organic pollutants.

Acknowledgements

This work is funded by the Ministry of Education and Training under grant no. B2022-TDV-06.

Conflict of Interests

The authors declare that they have no conflicts of interest.

Data Availability Statement

The data that support the findings of this study are available on request from the corresponding author According to reviewers' commments we revised the manuscript and we confirm that all information are correct.

Keywords: Akaline hydrothermal treatment · g-C_3N_4 · 2,4-D photodegradation · visible light irradiation · mechnism

[1] F. Islam, J. Wang, A. F. Muhammad, S. S. K. Muhammad, L. Xu, J. Zhu, M. Zhao, S. Muños, Q. X. Li, W. Zhou, *Environ. Int.* **2018**, *111*, 332–351.
[2] B. K. Jung, Z. Hasan, S. H. Jhung, *Chem. Eng. J.* **2013**, *234*, 99–105.
[3] X. Bian, J. Chen, and R. Ji, *Materials* **2013**, *6*, 1530–1542.
[4] A. M. Cupples, G. K. Sims, *Soil Biol. Biochem.* **2007**, *39*, 232–238.
[5] M. Golshan, B. Kakavandi, M. Ahmadi, M. Azizi, *J. Hazard. Mater.* **2018**, *359*, 325–337.
[6] J. S. Calisto, I. S. Pacheco, L. L. Freitas, L. K. Santana, W. S. Fagundes, F. A. Amaral, S. C. Canobre, *Heliyon* **2019**, 5, e02553.
[7] T. P. A. Shabeer, A. Saha, V. T. Gajbhiye, S. Gupta, K. M. Manjaiah, E. Varghese, *Environ. Technol.* **2014**, *35*, 2619e2627.
[8] A. Adak, I. Das, B. Mondal, S. Koner, P. Datta, L. Blaney, *Emerg. Contam.* **2019**, *5*, 53e60.
[9] K. H. H. Aziz, H. Miessner, S. Mueller, A. Mahyar, D. Kalass, D. Moeller, I. Khorshid, M. A. M. Rashid, *J. Hazard Mater.* **2018**, *343*, 107e111.
[10] D. Ma, H. Yi, C. Lai, X. Liu, X. Huo, Z. An, L. Li, Y. Fu, B. Li, M. Zhang, L. Qin, S. Liu, L. Yang, *Chemosphere* **2021**, *275*,130104.
[11] M. Zhang, H. Dong, L. Zhao, D. Wang, D. Meng, *Sci. Total Environ.* **2019**, *670*, 110–121.
[12] Y. Peng, X. Shen, L. Wang, B. Tian, Y. Liu, H. Chen, J. Lei, J. Zhang, *RSC Adv.* **2017**, *7*, 45742–4574.
[13] L. Yang, L. Wang, M. Xing, J. Lei, J. Zhang, *Appl. Catal. B* **2016**, *180*, 106–112.
[14] J. Yu, S. Wang, J. Low, W. Xiao, *Phys. Chem. Chem. Phys.* **2013**, *15*, 16883–16890.
[15] C. Dong, M. Xing, J. Zhang, *J. Phys. Chem. Lett.* **2016**, *7 (15)*, 2962–2966.
[16] K. A. Davis, S. Yoo, E. W. Shuler, *et al., Nano Converg.* **2021**, *8*, 6. https://doi.org/10.1186/s40580-021-00256-9.
[17] C. B. Anucha, I. Altin, E. Bacaksiz, V. N. Stathopoulos, *Chem. Eng. J. Adv.* **2022**, *10*, 100262.
[18] C. B. Ong, L. N. Yong, A. W. Mohammad, *Renewable Sustainable Energy Rev.* **2018**, *(81) 1*, 536–551.
[19] J. Wen, J. Xie, X. Chen, X. Li, *Appl. Surf. Sci. B* **2017**, *391*, 72–123.
[20] S. Wudil, U. F. Ahmad, M. A. Gondal, A. A. Mohammed, Al-Osta, A. Almohammedi, R. S. Sa'id, F. Hrahsheh, K. Haruna, M. J. S. Mohamed, *Arab. J. Chem.* **2023**, *(16,)3*, 104542.
[21] O. H. Abuzeyad, A. M. El-Khawaga, H. Tantawy, M. A. Elsayed, *Mol. Struct.* **2023**, *1288*, 135787.
[22] A. Esrafili, M. Salimi, A. J. Jafari, H. R. Sobhi, M. Gholami, R. R. Kalantary, *Mol. Liq.* **2022**, *352*, 118685.
[23] J. Gomes, J. Lincho, E. Domingues, R. M. Quinta-Ferreira, R. C. Martins, *Water* **2019**, *(11, 2)*, 373.
[24] N. Turkten, M. Bekbolet, *J. Photochem. Photobiol. A* **2020**, *401*, 112748.
[25] R. Acharya, K. Parida, *J. Environ. Chem. Eng.* **2020**, *(8 4)*, 103896.
[26] D. T. N. Hoa, N. T. T. Tu, H. Q. A. Thinh, L. V. T. Son, L. Vu. T. Son, N. D. V. Quyen, L. L. Son, T. N. Tuyen, P. L. M. Thong, L. H. Diem, D. Q. Khieu, *J. Nanomater.* **2023**, *9967890*, 15.
[27] A. B. Naveed, A. Javaid, A. Zia, M. T. Ishaq, M. Amin, Z. U. F. Rahman, and A. Mahmood, *ACS Omega* **2023**, *(8 2*, 2173–2182.
[28] L. Zhou, L. Wang, J. Zhang, J. Lei, Y. Liu, *Res. Chem. Intermed.* **2017**, *43*, 2081–2101.
[29] A. Q. Muhammad, M. Javed, S. Shahid, M. Shariq, M. M. Fadhali, S. K. Ali, M. S. Khan, *Heliyon* **2023**, *(9 1)*, e12685.
[30] O. Iqbal, H. Ali, N. Li, A. I. Al-Sulami, K. F. Alshammari, H. S. M. Abd-Rabboh, Y. Al-Hadeethi, I. U. Din, A. I. Alharthi, R. Altamimi, A. Zada, Z. Wang, A. Hayat, M. Z. Ansari, *Mater. Today Phys.* **2023**, *34*, 101080.
[31] H. Zhu, X. Yang, M. Zhang, Q. Li, J. Yang, *Mater. Res. Bull.* **2020**, *125*, 110765.
[32] M. A. Alcudia-Ramos, M. O. Fuentez-Torres, F. Ortiz-Chi, C. G. Espinosa-Gonz alez, N. Hern andez-Como, D. S. García-Zaleta, M. K. Kesarla, J. G. Torres-Torres, V. Collins-Martínez, S. Godavarthi, *Ceram. Int.* **2020**, *46*, 38–45.
[33] R. Acharya, K. Parida, *J. Environ. Chem. Eng.* **2020**, *8*, 103896.
[34] N. Madima, K. K. Kefeni, S. B. Mishra, A. K. Mishra, *Heliyon* **2022**, *8*, e10683.
[35] R. A. Senthil, J. Theerthagiri, A. Selvi, J. Madhavan, *Opt. Mater.* **2017**, *64*, 533–539.
[36] Y. Tan, Z. Shu, J. Zhou, T. Li, W. Wang, Z. Zhao, *Appl. Catal. B* **2018**, *230*, 260–268.
[37] S. Yurdakal, S. Çetinkaya, V. Augugliaro, G. Palmisano, J. Soria, J. Sanz, M. J. Torralvo Fernández, S. Livraghi, E. Giamello, C. Garlisi, *Catal. Sci. Technol.* **2020**, *10*, 5000–5012.
[38] T. Kasuga, M. Hiramatsu, A. Hoson, T. Sekino, K. Niihara, *Langmuir* **1998**, *14*, 3160–3163.
[39] R. Camposeco, S. Castillo, J. Navarrete, R. Gomez, *Catal. Today* **2016**, *V.266*, p. 90–101.
[40] M. A. L. Zavala, S. A. L. Morales, M. A. Santos, *Heliyon* **2017**, *3*, e00456.
[41] S. Yurdakal, S. Çetinkaya, V. Augugliaro, G. Palmisano, J. Soria, J. Sanz, M. J. Torralvo Fernández, S. Livraghi, E. Giamello, C. Garlisi, *Catal. Sci. Technol.* **2020**, *10*, 5000–5012, DOI: 10.1039/D0CY00755B.
[42] N. D. Shcherban, P. Mäki-Arvela, A. Aho, S. A. Sergiienko, P. S. Yaremov, K. Eränenb and D. Yu. Murzin, *Catal. Sci. Technol.* **2018**, *8*, 2928–2937.
[43] L. Zhang, H. Wang, W. Shen, Z. Qin, J. Wang, W. Fan, *J. Cat.* **2016**, *344*, 293–302.
[44] J. Li, M. Zhang, Q. Li, J. Yang, *Appl. Surf. Sci.* **2017**, *391*, 184–193.
[45] M. Roškarič, G. Žerjav, M. Finšgar, J. Zavašnik, A. Pintar, *J. Alloys and Compd.* **2023**, *947*, 169585.
[46] J. Zhang, W. Yu, J. Liu, and B. Liu, *Appl. Surf. Sci. A* **2015**, *358*, 457–462.
[47] N. T. T. Ha, P. T. Be, P. T. Lan, N. T. Mo, L. M. Cam, N. Ha, *RSC Adv.* **2021**, *11*, 16351–16358.
[48] R. Hao, G. Wang, H. Tang, L. Sun, C. Xu, D. Han, *Appl. Catal. B* **2016**, *187*, 47–58.
[49] F. J. Sotomayor, K. A. Cychosz, M. Thommes, *Acc. Mater. Surf. Res.* **2018**, *3 (2)*, 34–50.
[50] R. Kumar, M. A. Barakar, B. A. Al-Mur, *J. Clean. Prod.* **2020**, *246*, 119076.
[51] M. Hepel, J. Luo, *Electrochim. Acta.* **2001**, *47*, 729–740.
[52] A. Toghan, H. M. Abd El-Lateef, K. K. Taha, A. Modwi, *Relat. Mater.* **2021**, *118*, 108491.
[53] L. Ma, G. Wang, C. Jiang, H. Bao, Q. Xu, *Appl. Surf. Sci.* **2018**, *430*, 263–272.
[54] S. Ni, Z. Fu, L. Li, M. Ma, Y. Liu, *Colloids Surf. A Physicochem. Eng. Asp.* **2022**, *649*, 129475.
[55] B. Chai, T. Peng, J. Mao, K. Li, L. Zan, *Phys. Chem. Chem. Phys.* **2012**, *14*, 16745–16752.
[56] H. Ji, F. Chang, X. Hu, W. Qin, J. Shen, *Chem. Eng. J.* **2013**, *218*, 183–190.
[57] R. Liu, Y. Liu, C. Liu, S. Luo, Y. Teng, L. Yang, R. Yang, Q. Cai, *J. Alloys and Compd.* **2011**, *509*, 2434–2440.
[58] D. F. Ollis, *Environ. Sci. Technol.* **1985**, *(19 6)*, 480–484.
[59] A. H. Balakrishnan, K. Gopalram, S. Appunni, *Environ. Sci. and Pollu. Research* **2011**, *28*, 33331–33343.

Manuscript received: December 13, 2023